

Modeling with the FDTD Method for Microwave Breast Cancer Detection

ABSTRACT

This paper addresses important issues related to finite-difference time-domain modeling for microwave breast cancer detection. we present a simple and efficient way of modeling dispersion for various types of biological tissue, in the range of 30 mhz–20 ghz. propagation and absorbing boundary conditions are modified accordingly. results from three-dimensional simulations of a semiellipsoid geometric representation of the breast terminated by a planar chest wall illustrate the effect of certain important aspects of the detection problem including: 1) the pulse distorting effects of propagation in frequency-dependent tissue; 2) the choice of the surrounding medium; and 3) the transmitter location relative to the breast and chest wall. In particular, it is shown that the presence of the chest wall can affect greatly the system's detection abilities, even for tumors that are not located in the proximity of the chest wall. index terms—breast cancer detection, dispersive media, finite difference time domain (fdtd), microwave imaging.

Keywords: Breast cancer detection, dispersive media, finite difference time domain (FDTD), microwave imaging

1. Introduction

MICROWAVE imaging for breast cancer detection has recently attracted the interest of many researchers as a promising new technique, which may be able to overcome some of the shortcomings of X-ray mammography. It is based on recently published data [1–4], which reveals an important difference in the electromagnetic properties of malignant tumor tissue relative to normal fatty breast tissue with a ratio that can reach one order of magnitude. As further measurements aiming to describe the electromagnetic properties of the breast continue, microwave imaging systems, which aim to detect and localize tumors in the breast, are being developed.

In active microwave imaging, two different techniques have achieved promising results in simulations and laboratory experiments [5]. The first technique aims to recover the breast electrical properties based on near-field tomographic image reconstruction algorithms [6,7]. Meaney *et al.* [8] have achieved encouraging results with simulation and phantom data, as well as some preliminary clinical exams. The second technique is based on backscattered data collected by antennas placed in different positions, and uses an ultrawide-band (UWB) pulse to excite the transmitting antenna. The confocal microwave imaging (CMI) technique was first introduced by Hagness *et al.* [9,10]. In [11], a two-dimensional (2-D) imaging algorithm based on a planar geometry was proposed and tested for magnetic resonance imaging (MRI)-based simulation data, whereas a cylindrical CMI system has also been presented and analyzed with simulation data [12]. Using three-dimensional (3-D) simula-

tions and simple 3-D breast models, it was also shown that the two systems lead to similar performance [13]. Experimental results that examine the feasibility of the cylindrical CMI system have also been reported [14]. Recently, a method based on space-time beamforming, which overcome some of the shortcomings of previous CMI algorithms, was also proposed [15], and encouraging experimental results with breast and tumor tissue phantoms have been presented [16].

As time-domain microwave breast imaging algorithms are usually based on numerical simulations with the finite-difference time-domain (FDTD) method [17], accurately modeling all the different aspects of the problem is very important for the evaluation of these systems. Biological tissue in general is quite dispersive in the microwave frequency range. Modeling of the frequency dependence for the various types of tissue is an important challenge for time-domain analysis of microwave breast cancer detection systems. Our goal in this paper is to suggest a simple and efficient way of incorporating dispersion based on data for the frequency range of 30 MHz–20 GHz. We develop a 3-D FDTD model that incorporates dispersion in order to study the effect of certain parameters of the detection problem, such as source location relative to the chest wall, and the effect of the surrounding medium to the backscattered signal from the system.

This paper is organized as follows. First, we present an accurate and efficient way of modeling dispersion for various biological tissues. Using the example of disper-

sive breast fat, we compare the accuracy of the proposed method to first-order Debye models that have appeared in the literature, and discuss the advantages and shortcomings of these two approaches. We also develop a novel implementation of the uniaxial perfectly matched layer (UPML) absorbing boundary condition (ABC), which can be used to account for such dispersive media. We then present 3-D FDTD simulations with a semiellipsoid breast model, terminated with a chest wall. Comparison of results for nondispersive and dispersive modeling for the tissues illustrates the importance of including dispersion for the accurate prediction of the system's response. We also examine the effect of the surrounding medium to the level of clutter and the dynamic range of the system. Finally, it is shown that the presence of the chest wall can obscure detection if the source is located close to the chest wall.

2. FDTD Modeling of Dispersive Biological-Tissue

For frequency-dependent FDTD modeling of electrically dispersive media, three general approaches have been proposed in the literature. The recursive convolution (RC) approach [18] implements a discrete convolution with a recursive summation by approximating the complex permittivity with a sum of first order poles in frequency. On the other hand, the auxiliary differential (ADE) approach [19,20] uses an auxiliary differential equation relating the electrical displacement D to the electric field E . Finally, in the Z -transform approach [21], the time-domain convolution is reduced to a difference equation via Z -transform theory. These three methods have been used to model Debye or Lorentz media, and extensions of the methods to arbitrary dispersive media, such as [22] for the RC and [23] for the Z -transform approach, have also been developed. Good results have been obtained with all three methods, with some differences in the accuracy, the computational cost and the implementation specifics of each approach.

For biological tissue, the most popular approach for handling dispersion has been to model the medium with a multiterm Debye relaxation equation and use the ADE method to obtain a time-domain equation between $D(t)$ and $E(t)$ [19]. To maintain the method's implementation simplicity and reduce its computational cost, a ceptable fit to measured data must be achieved for Debye models of the first or second order. Thus far, a single-pole Debye equation, with parameters chosen to fit published data up to 3 GHz [9], [11,15], has been used for FDTD breast tumor scattering simulations. In this study, we extend breast tissue models reported in the literature to accurately consider frequency-dependent dispersion beyond 3 GHz, based on measured values up to 20 GHz [24]. This is essential in order to resolve small tumors in very dispersive breast tissue using high spatial resolution impulses with frequency content that can extend up to 12 GHz. We propose a different way of incorporating dis-

persion in the FDTD models based on the Z -transform approach and previous work on time-domain modeling of dispersive soil, and compare the accuracy and efficiency of this approach to the standard first-order Debye model.

For certain types of media, such as soil and biological tissue, the lossy dispersive wave equation is governed almost entirely by the frequency-dependent conductivity. The frequency variation of the real dielectric constant does not significantly affect either the real propagation constant β or the decay rate α . Based on this observation, a model that captured the entire dispersive behavior of dispersive soil by fitting conductivity parameters was developed in [25]. In particular, a two-pole rational function of the Z -transform $Z = e^{j\omega\Delta t}$ for FDTD time step was used to approximate the conductivity. In [26], it was further shown that a single-pole conductivity model is sufficient for good agreement with dispersive soil data over a decade of frequency. The accuracy of the method has been tested by comparing the soil response calculated by the FDTD model with measured data in a ground penetrating radar experiment, leading to very good agreement [27]. Here, we follow this approach to derive models for various types of dispersive biological tissue. Using the single-pole conductivity model,

$$\sigma(Z) = \frac{b_0 + b_1 + b_2 Z^{-2}}{1 + a_1 Z^{-1}} \quad (1)$$

Ampere's law can be written in the Z -domain as

$$\nabla \times \mathbf{H}(Z) = \varepsilon_{av} \varepsilon_0 \frac{1 - Z^{-1}}{\nabla t} \mathbf{E}(Z) + \sigma(Z) \mathbf{E}(Z) \quad (2)$$

where ε_{av} is frequency independent. We should note here that, in (2), we choose to consider only the current density value, while in previous development of the method, we used an average of the current and past values. The current choice leads to memory savings and simpler stability analysis, while the loss in accuracy is within the error of the fit of the dispersive model to the data, as demonstrated with different types of soil in [26]. Substituting (1) into (2) and then converting back into the time domain, keeping in mind that Z^{-1} represents a time delay, the FDTD propagation equations are readily available. For example, for a 2-D TM_z FDTD simulation, the necessary equations have the form,

$$E_z^{n+1} = -\frac{1}{e_o} (e_1 E_z^n + e_2 E_z^{n-1} + \Delta H_x - \Delta H_y) \quad (3)$$

$$\Delta H_\gamma = \frac{\Delta t}{\varepsilon_{av} \varepsilon_0} \left(I_\gamma^{n+\frac{1}{2}} + a_1 I_\gamma^{n-\frac{1}{2}} \right), \quad \gamma = x, y \quad (4)$$

where

$e_o = 1 + (b_o \Delta t / \varepsilon_{av} \varepsilon_0)$, $e_1 = a_1 - 1 + (b_1 \Delta t / \varepsilon_{av} \varepsilon_0)$, $e_2 = -a_1 + (b_2 \Delta t / \varepsilon_{av} \varepsilon_0)$ and I_x , I_y are the spatial first differences of the magnetic-field components H_x and H_y with respect to y and x . We should note that we choose to present (3) and (4) separately for clarity while,

in fact, they can be combined into one single equation, which updates the current electric-field value using the two previous ones and the current and previous magnetic-field value.

It is clear from (1) that conductivity depends on frequency, time step Δt , and the parameters a_1 , b_0 , b_1 , and b_2 . The rational function (1) also contributes to the real dielectric constant. Thus, to solve for the model parameters, the resulting conductivity and dielectric constant for the model and measured data are equated at three representative frequencies. For the solution, an initial guess is made for a_1 , and optimization can be performed with a simple trial-and-error procedure. Due to the infinite impulse response (IIR) filter-type equation (1) for σ , the stability analysis of this dispersion algorithm is nontrivial, and can be derived from the more general analysis presented in [23] based on the Von Neumann stability criterion. The resulting dispersive stability condition for a source-free medium can be described by [28]

$$(Z-1)e_{av} \frac{e_0 + e_1 Z^{-1} + e_2 Z^{-2}}{1 + a_1 Z^{-1}} + \frac{12c^2 \Delta t^2}{\varepsilon_{av} \Delta_2} = 0 \quad (5)$$

To ensure stability, all three (complex) Z -values that are roots of (5) must lie within the unit circle. This requirement results to a minimum value of the spatial step

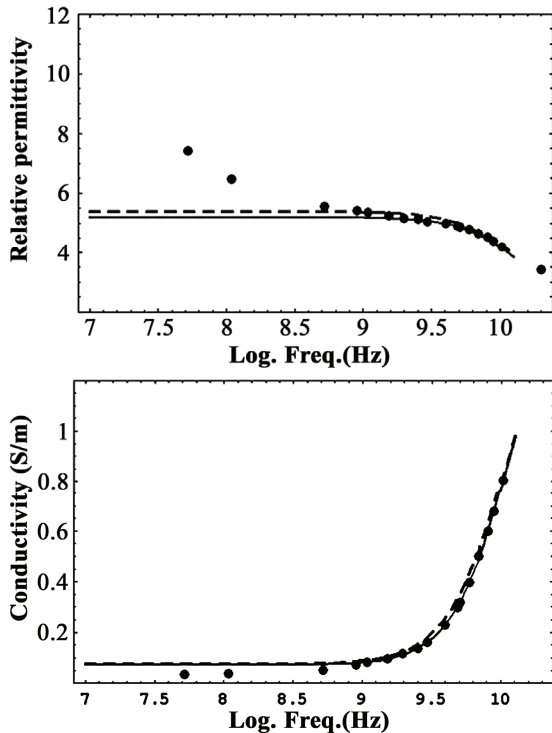


Figure 1. Plots of the: (top) relative permittivity and (bottom) conductivity in siemens per meter as a function of the logarithmic frequency. The solid lines represent values predicted by the single-pole conductivity model, the dashed lines by the present Debye model, and the black dots by measured human breast fat data at 37° C [24]

size Δ , which can be larger than the smallest step size resulting from the usual Courant condition for the given medium. The upper bound on the sampling interval Δ obeys to the standard rule of $\Delta_{\max} \leq (\lambda/10)$. More details on the derivation and stability analysis of these dispersion comparisons of this model to the first-order Debye model, which has been employed for FDTD modeling of microwave breast cancer detection.

To compare the above model with the ADE approach via a Debye first-order equation, we first examine the agreement of each with measured data for normal breast fat tissue, provided by [24] for the frequency range of 30 MHz–20 GHz. Since the Debye parameters in [9] were chosen to fit to different data [2] for frequencies up to 3 GHz, we derived a new Debye first-order model of the form

$$\varepsilon_r(\omega) - j \frac{\sigma(\omega)}{\omega \varepsilon_0} = \varepsilon_\infty + \frac{\varepsilon_s - \varepsilon_\infty}{1 + j\omega\tau} - j \frac{\sigma_s}{\omega \varepsilon_0} \quad (6)$$

with $\varepsilon_\infty = 2.8$, $\varepsilon_s = 5.4$, $\sigma_s = 0.075$ S/m, and $\tau = 14.0$ ps. The coefficients for the single-pole conductivity model at $\Delta t = 2$ ps are $a_1 = -0.8785$, $b_0 = 11.257$, $b_1 = -2.0105$, and $b_2 = 8.855$ and the average permittivity is $\varepsilon_{av} = 0.94$. In Figure 1, we plot the conductivity and relative permittivity for the two models and the measured data as functions of frequency on a logarithmic scale, while in Figure 2, the real propagation constant β and decay rate α are plotted. Also plotted in Figure 2 are the

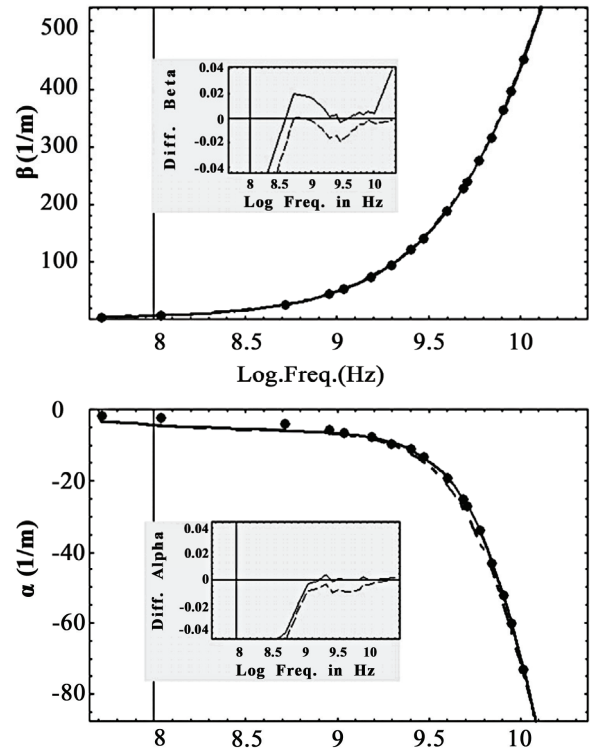


Figure 2. Same as Figure 1, for the: (top) real and (bottom) imaginary parts of the wavenumber k (meter units). The insets show the corresponding normalized errors

normalized errors in phase velocity and decay rate. These plots show that the two models have similar fits to the measured permittivity and conductivity, but the single-pole conductivity model is more accurate in representing the attenuation factor α . The normalized error for β is below 2% for both models in the frequency range of 1–13 GHz, while the error for α in the same range is significantly smaller for the single-pole conductivity model. Since α and β represent the real and imaginary parts of the wavenumber k , they are the most important measures of the models' accuracy.

In terms of stability, the analysis presented above, applied to the breast fat model, results in a $\Delta_{\min} = 0.57$ mm. A similar stability analysis for the Debye model [29] shows that stability is ensured for $\Delta > (c_0 \Delta t / \sqrt{\epsilon \infty})$, which yields $\Delta_{\min} = 0.36$ mm. For the single-pole conductivity model, each value of the time step Δt determines a unique set of the fitting parameters, as well as the limits on the spatial step Δ . This appears to be a disadvantage of this model relative to the Debye equation, where the choice of the fitting parameters is independent of the time step. One should keep in mind, however, that a restriction on the choice of the time step in an FDTD algorithm, which uses the ADE method, is also imposed since it should be of the order of $O(10^{-3} \tau)$, where τ is the model's relaxation constant, in order to ensure accurate results [29]. Furthermore, the presence of the additional auxiliary equation does not preserve the nondissipative character of the standard FDTD algorithm and, therefore, accuracy is ensured when the spatial step Δ is chosen to be close to its Courant limit [29]. In terms of memory requirements, the FDTD implementation for the model described by (1) requires storage of one additional value per electric and magnetic-field components, while the first order Debye model requires storage of the current density \mathbf{D} . The Debye model is computationally more expensive relative to the single-pole conductivity model since it requires an extra computation for each component due to the auxiliary equation.

As with the propagation equations, ABCs can also be modified in a way to account for dispersion using the single-pole conductivity model. In [30], an ABC based on this model and the one-way wave equation was proposed, leading to acceptable reflection less than 1% for lossy dispersive media. Here, we present a new way of implementing the UPML [31] for dispersive media, which can be described with the single-pole conductivity model, which was analyzed above. Our formulation is a simple extension of the UPML theory for termination of conductive media, as it is presented in [17]. Keeping the same notation as in [17], the update of any electric-field component in the UPML medium can be described by a system of equations as follows for E_z for an ABC at $z = z_{\max}$:

$$\partial_z H_y - \partial_y H_x = \epsilon \partial_t P'_z + \sigma P'_z \quad (7)$$

$$\partial_t P'_z = \partial_t (k_x P_z) + \frac{1}{\epsilon_0} \sigma_x P_z \quad (8)$$

$$\partial_t (k_z P_z) + \frac{\sigma_z}{\epsilon_0} P_z = \partial_t (k_y E_z) + \frac{\sigma_y}{\epsilon_0} E_z \quad (9)$$

respect to x , y , and t , respectively. To avoid confusion, we note that α in (7) is the actual conductivity of the lossy medium, while σ_n , $n = x, y$, and z in (8) and (9) are the perfectly matched layer (PML) conductivities. While this formulation has been used for lossy media with constant conductivity σ , it can be easily extended to dispersive media by realizing that (7) converted in the \mathbf{Z} -do-main is identical to (2) for $\epsilon(Z) = \epsilon_{av}$ and $\sigma(Z)$ the single-pole conductivity model (1). Therefore, the dispersive UPML formulation that we use is described by the system of (3), (8), and (9) with E_z replaced by P'_z in (3). The magnetic-field equations in the UPML medium are, of course, identical to those of the original formulation for free space.

To test the performance of this novel UPML implementation for the dispersive breast fat model that was presented above, we examined absorption of a normally incident plane wave TM_z excited with a modulated Gaussian pulse of 8-GHz central frequency. Fig. 3 shows the resulting reflection coefficient observed one cell away from the UPML boundary. The reflection coefficient was where ∂_x , ∂_y , and ∂_t denote partial derivatives with calculated as $R(\text{dB}) = 20 \log_{10} |F\{E'_z(t) - E^i_z(t)\}| / |F\{E^t_z(t)\}|$ with F denoting the Fourier transform and E^t and E^i denoting the total and incident fields, respectively. From this figure, we see that the performance of the method is similar to previous results for various implementations of the PML in dispersive media [32,33]. For a ten-layer UPML, the reflection ratio is around -90 dB for the frequency range of 100 MHz–15 GHz. The reflection coefficient for a lossy nondispersive medium of electric properties calculated from the dispersive model at the central frequency of 8 GHz is also plotted for comparison, and is almost identical to the dispersive case. Thus, it is clear that incorporating dispersion in the UPML does not affect performance. In terms of memory requirements, the UPML implementation needs the same amount of additional storage relative to the propagation equations as previous UPML formulations for dispersive media [32]. These additional memory requirements were calculated to be 16% for an N^3 grid with $N = 100$ [30].

3. 3-D FDTD Simulations for Breast Cancer Detection

Using the approach presented above, we develop a

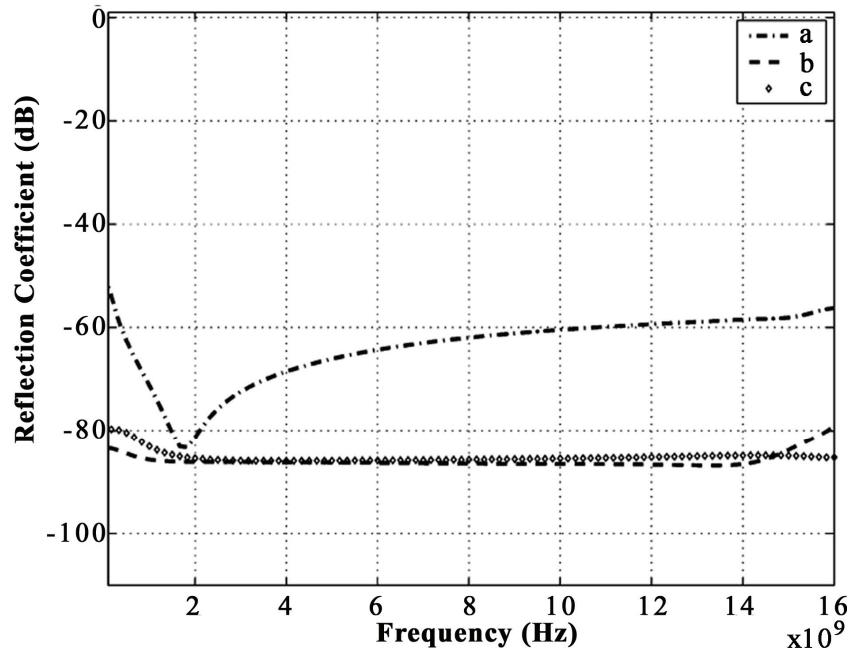


Figure 3. Reflection coefficient for the UPML medium implemented with the single-pole conductivity model of (1), terminating dispersive breast fat tissue with dispersion characteristics shown in Figure 1. Reflection is observed one cell away from: (a) four and (b) ten UPML layers. For comparison, the result for ten layers and nondispersive breast fat with constant σ is also plotted in (c)

3-DFDTD model in order to examine some important aspects of UWB microwave breast cancer detection, such as the choice of the surrounding medium and the reflections from the chest muscle. In connection with Section II, we compare results from dispersive and nondispersive FDTD algorithms in order to quantify the effect of dispersion in the prediction of the system's response to UWB excitation pulses. In addition, we examine how various surrounding media affect dynamic range and clutter, and study how the reflections from the skin, breast, and chest wall can affect the system's detection abilities for different source locations.

In all our simulations, the breast boundary is given by the equation of a 3-D semiellipsoid $(x/8.3)^2 + (y^2 / 5.7^2) + (z^2 / 5^2) = 1, z \geq 0$ with axes units of centimeters and the tumor is modeled as a 4-mm-diameter sphere of high water content (HWC) tissue. The breast is filled with normal breast fat and is bounded by a skin layer of 2-mm thickness. To incorporate regions in the breast with higher electric properties corresponding to fibroglandular tissue, we consider a concentric hemispherical region of radius 4.5 cm, with tissue 27% higher permittivity and 30% higher conductivity than the normal breast fat. These values were chosen as an upper bound on the variability in the normal breast tissue properties that has been

observed [34]. Although not completely realistic, the hemispherical region was chosen based on real MRI scans of the breast showing that fibroglandular regions appear to be highly correlated, rather than randomly distributed in the breast [35].

3.1. Fully Dispersive Tissue Simulation

An example of the spatial field distributions of our simulation results is shown in Figure 4. A Hertzian dipole source is modeled with a single point of the FDTD grid excited with an electric field E_z using an ideal broad-band Gaussian pulse modulated at the central frequency of 8 GHz with a 3-dB bandwidth extending up to 13 GHz. At first, the source coordinates are chosen at (0.0, -5.0) for the horizontal and vertical positions, respectively, and the height is 4.5 cm above the chest wall. The surrounding medium for this simulation has been chosen to be a synthetic nondispersive lossy dielectric with $\epsilon_r = 4.48$ and $\sigma = 0.59$ S/m. These values match closely, but not perfectly, the nominal values of the electric properties of the dispersive breast fat model at 8 GHz, which are 4.58 and 0.52 S/m, respectively. The grid cell size is $\Delta = 0.57$ mm and the time step $\Delta_t = 2$ ps. All tissues in this simulation are considered dispersive and modeled using (1) and data from [24]. The malignant tumor is modeled as general HWC tissue. The dispersive model parameters for all tissue types are given in Table 1.

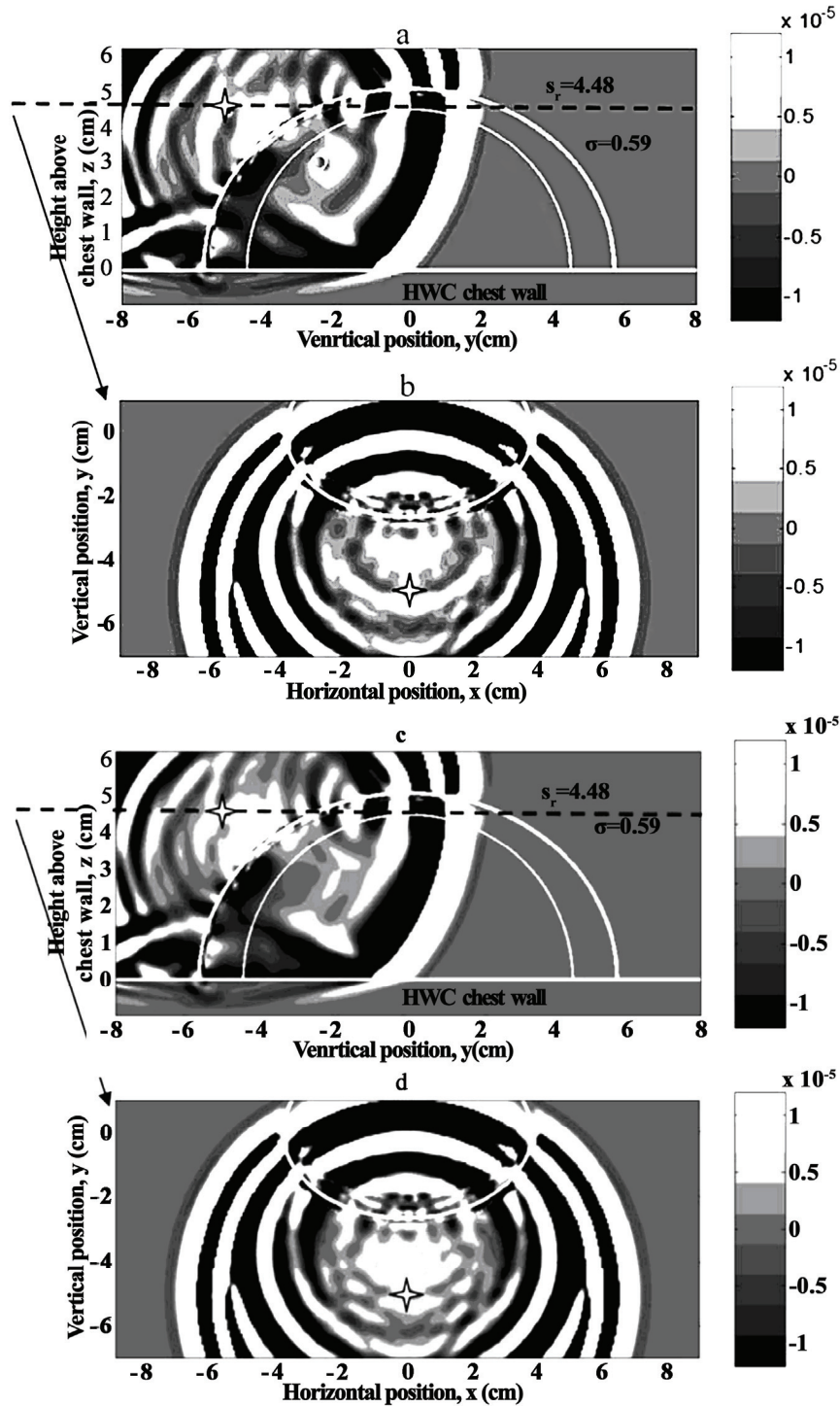


Figure 4. Spatial distribution of the electric field E_z at $t=620\text{ps}$ due to a source (marked with a white cross) at $(0, -5.0, 4.5)$ in the presence of a 4-mm-diameter tumor (marked with a white circle) at $(0, -2.5, 3.0)$. (a) Breast axial view through the center of the tumor. (b) Coronal view through the plane of the source. The same case without the tumor is plotted for comparison in (c) and (d). The signal scattered from the tumor is visible with careful inspection as a white arc in the area behind the source

3.2. Dispersion Effect

The effect of dispersion in the tumor response was first examined by Hagness *et al.* in [9]. Using a double-sideband (DSB) 6-GHz modulated Gaussian pulse, no degradation in the signal-to-clutter ratio for dispersive

relative to nondispersive modeling results was observed. This result was attributed to the symmetry of the excitation pulse and the effect of the time-shift and summation technique for their particular system configuration. Our study does not focus on a particular detection system, but rather examines the effect of dispersive modeling in the

general prediction of the breast-tumor response to an UWB pulse of very high-frequency content.

To quantify the importance of including dispersion in the FDTD models, we simulated the previous FDTD case of Figure 4, considering all tissues as nondispersive, using constant values for the permittivity and conductivity calculated from the dispersive models at the central frequency of 8 GHz. To simplify the comparison, no fibroglandular region was considered in these simulations. The late time electric field E_z observed near the transmitter at (0, -5.5, 4.5) cm for the dispersive and nondispersive models is plotted in Figure 5. It is clear that modeling the frequency dependence of tissue is essential for predicting both the shape and magnitude of the system's response. The backscattered signal from the tumor is visible for a much longer time interval in the nondispersive model, and with considerably greater magnitude relative to the tumor-free response. In the time interval of interest, the maximum power of the tumor response for the nondispersive model is 7.5 dB higher than the power in the absence of the tumor, while for the dispersive case, it is only 1.7 dB higher. In addition, pulse-shape distortions for dispersive tissue signals are great enough to alter important detection features. Note that a zero crossing of dispersive tissue tumor/no-tumor difference occurs at 650 ps, which is one of the maxima of the corresponding nondispersive difference.

3.3. Effect of the Surrounding Medium

In previous UWB microwave detection systems, surrounding materials that either match the properties of the skin or the normal breast fat have been proposed. For a transmitter located further away from the breast, reflections from the skin are less significant than for antennas adjacent to the breast, but loss in the surrounding medium may raise the required dynamic range of the receiver. To study the effect of the surrounding medium, we repeated the simulation presented in Figure 4, comparing clutter and dynamic range for different materials. As we are interested in the breast/skin and tumor response in relation to the different media, the fibroglandular region has been omitted. In addition to the lossy dielectric of $\epsilon_r = 4.48$ and $\sigma = 0.59$ S/m, we considered a lossless dielectric with the same ϵ_r , as well as vaseline with $\epsilon_r = 2.16$ and $\sigma = 0.01$ S/m. For the same source location as in Figure 4, we calculated the maximum power of the tumor response (S) relative to the maximum incident power (T) at the observation point, S/T , as well as relative to the reflected signal to clutter (S/C) for two different observation points, one close to the source and one close to the tumor. The locations of these points and the corresponding results are shown in Table 2. A comparison of the power ratios for

Table 1 Parameters For The Dispersive Tissues Of The FDTD Model

Tissue	a_1	b_0	b_1	b_2	ϵ_{av}
Tumor	-0.8785	77.384	-129.99	52.74	6.04
Muscle	-0.8585	239.65	185.61	-425.1	-27.4
Breast fat	-0.8785	11.257	-20.105	8.855	0.94
Fibroglandular	-0.8917	11.43	-20.4	8.99	1.88
Skin	-0.8985	311.53	-584.1	272.66	-46.2

Table 2. Normalized Power Of Tumor Response For Different Surrounding Materials

Medium	(ϵ_r, σ)	Power ratio (dB) At (0,-5.5,4.5) (S/T,S/C)	Power ratio (dB) At (0,-6.2,3.0) (S/T,S/C)
Breast fat phantom	(4.48, 0.59)	(-86.6, -43.1)	(-64.1, -35.0)
Lossless phantom	(4.48, 0.0)	(-74.4, -43.5)	(-59.0, -36.0)
Vaseline	(2.16, 0.01)	(-75.3, -47.0)	(-59.8, -40.1)

the three different media shows the effect of the chest wall in the signal scattered from tumors in the proximity of that the impact of the surrounding material is relatively small; the lossy dielectric simulating breast fat leads to the highest S/C ratio, but also requires the greatest dynamic range of the sensor, in comparison to its lossless equivalent and the vaseline. The clutter caused by the skin is not very sensitive to the surrounding medium due to the high contrast in its electric properties relative to all three materials. The obvious advantage of a medium like vaseline is that it is readily available, while it does not significantly degrade the system's performance.

3.4. Reflections from Chest Wall

Chest muscle was studied for a planar geometry in [10], where it was shown that detection of the tumor is possible using a pair of perpendicular antenna elements forming a Maltese cross. In the current model, we use a semiellipsoidal breast geometry terminated with a planar chest wall. For such a geometry, the chest-wall reflections can obscure detection depending on the location of the source and the receiver relative to the tumor and chest wall, even if the tumor is located far from the chest wall. To illustrate the impact of the source location relative to the chest wall and tumor, we repeated the general simulation of Figure 4 for a source at (0, -5.7, 3.0) cm and a tumor at (0, -3.0, 3.0) cm. These source and tumor positions were chosen so that the source is closer to the tumor than in Fig. 4, but not adjacent to the breast. The spatial field distribution for the same time instant as in Fig. 4 is shown in Fig. 6. Comparison of the two figures shows that, while in both cases the overall clutter response is dominated by skin reflections, additional clutter of the same level as the tumor response occurs for the source location of Figure 6. The difference is clear if one compares the field distributions in the area near the source with and without the tumor. While in Figure 4 the difference in the signal due to the tumor is visible as a white

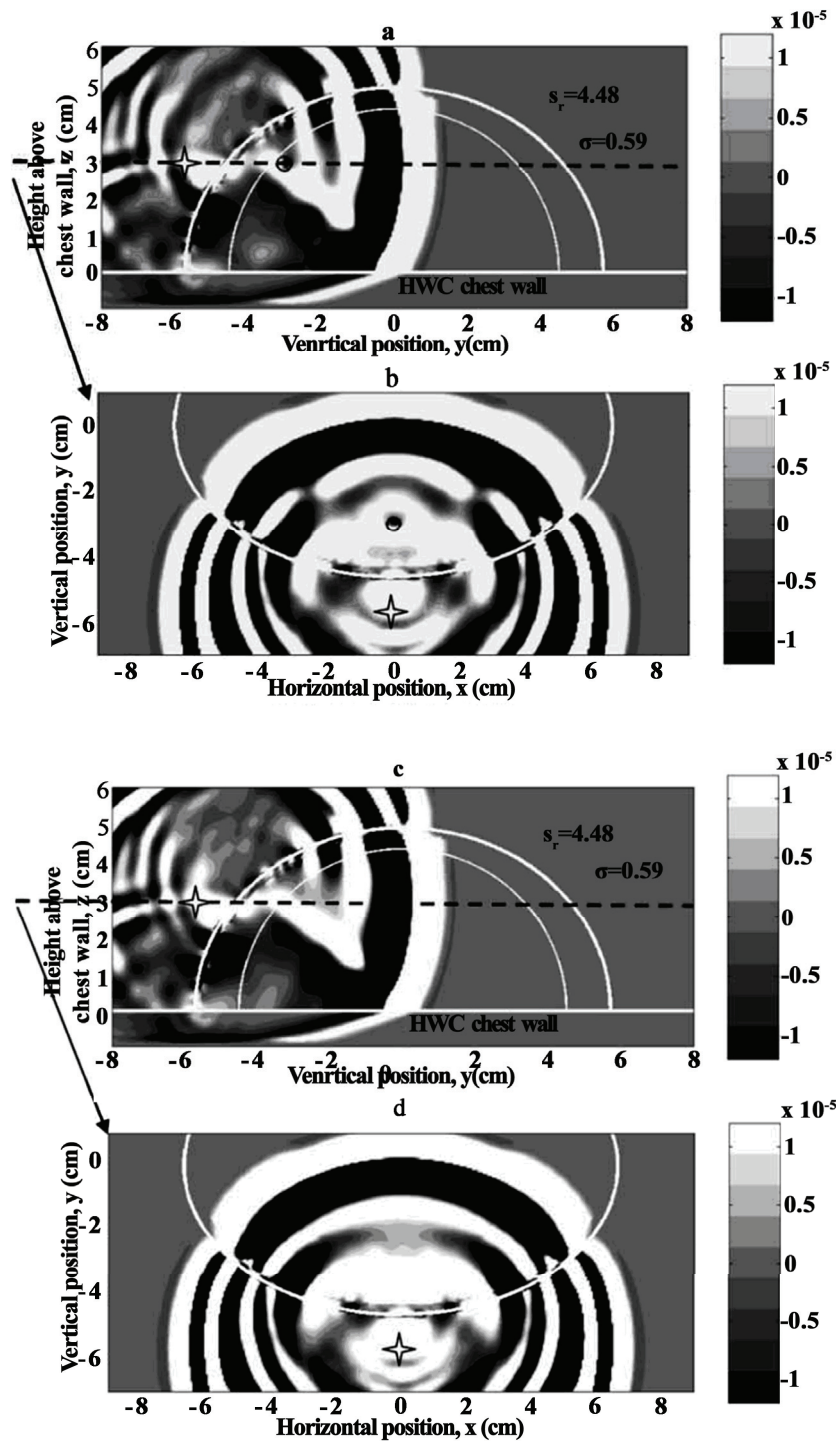


Figure 6. Same as Figure 4, but for a source located at $(y; z) = (-5; 7; 3; 0)$ cm and a tumor at $(y; z) = (-3; 0; 3; 0)$. The sensor is closer to the tumor than in Figure 4, but the tumor signal is obscured by reflections from the chest wall, which interfere with the tumor response in the area near the source

arc in the area behind the source, detecting any difference in the signal for the tumor and tumor-free case is very challenging for Figure 6. Although in the latter case a higher tumor response is expected due to the tumor being closer to the source, the additional reflections from the wall obscure the tumor signal. In a detection system, of

course, it will not be possible to distinguish clutter from the tumor response or the chest-wall reflections; what this study shows is that the inclusion of the chest wall in the FDTD model is necessary for an accurate prediction of the various sources of clutter that can obscure tumor detection. More importantly, these results suggest that a sys

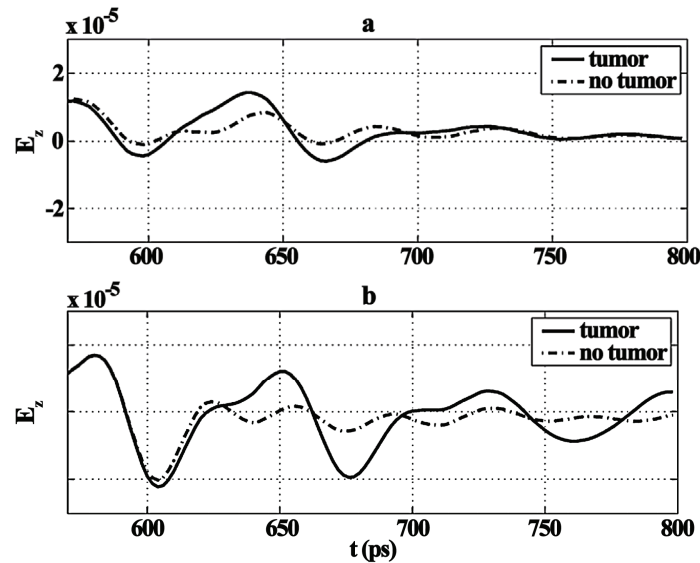


Figure 5. Comparison of the normalized reflected electric field (late time response) at $(y; z) = (-5; 5)$ cm as function of time for the geometry of Fig. 4 (without the fibroglandular region). (a) Dispersive model. (b) Nondispersive model with $\epsilon_r = 4.58$ and $\sigma = 0.52$ S/m for breast fat and $\epsilon_r = 39.0$ and $\sigma = 7.9$ S/m for the tumor

tem located at a distance from the chest wall may be preferable in order to minimize the chest-wall effect.

4. Summary and Conclusions

This paper's primary goal has been to present an alternative method for incorporating dispersion in FDTD modeling of UWB microwave breast cancer detection problems. Motivated by previous studies on time-domain modeling of dispersive soil, we developed a single-pole conductivity model, which can account for the frequency dependence of the electric properties for biological tissue in the range of 30 MHz–20 GHz, with particularly close agreement above 800 MHz. Tables that show good agreement of the model with data for various types of tissue can be found in [36]. As current research is concerned with microwave breast cancer detection applications, we focused on comparing our approach to Debye first-order models that have been previously employed. Using data for breast fat, we examined the accuracy of each model and discussed the advantages of each approach in terms of implementation, efficiency, and computational cost. An important feature of the models developed here is that they are based on data, which extends to 20 GHz, which is necessary for high-resolution detection systems. A way to modify the UMPL ABC using this dispersion model was also presented, showing performance similar to a lossy nondispersive formulation.

Based on the suggested approach, a fully dispersive 3-DFDTD model of a semiellipsoidal breast terminated with a chest wall was developed. Although we do not suggest a complete detection system, we identify several important aspects of the modeling problem. While the geometry is not fully realistic, this model incorporates many characteristic features of microwave breast cancer detection, such as wide tissue density variation, tumor

positioning in lower contrast medium, and chest-wall muscle inclusion. To illustrate the importance of considering dispersion for the accurate prediction of the system's response, the electric fields calculated from dispersive and nondispersive models were compared. In addition, the effect of the properties of the surrounding medium was studied, and it was shown that the clutter due to the skin is not particularly sensitive to the properties of the background medium. For sensors close to the chest wall, reflections from the muscle layer can interfere with the tumor signal and obscure detection, even for tumors that are not adjacent to the wall. Thus, modeling the chest wall is essential, and it is important to place the source at some distance from it in order to reduce its impact.

5. Acknowledgment

The authors would like to thank the reviewers for their invaluable remarks and suggestions.

REFERENCES

- [1] w. t. joines, y. z. dhenxing, and r. l. jirtle, "the measured electrical properties of normal and malignant human tissues from 50 to 900 mhz," *med. phys.*, vol. 21, pp. 547–550, 1994.
- [2] s. s. chaudhary, r. k. mishra, a. swarup, and j. m. thomas, "dielectric properties of normal and malignant human breast tissues at radiowave and microwave frequencies," *indian. j. biochem. biophys.*, vol. 21, pp. 76–79, 1984.
- [3] c. gabriel, s. gabriel, and e. corthout, "the dielectric properties of biological tissues: i. literature survey," *phys. med. biol.*, vol. 41, pp. 2231–2249, 1996.
- [4] s. gabriel, r. w. lau, and c. gabriel, "the dielectric properties of biological tissues: ii. measurements on the frequency range 10 hz to 20 ghz," *phys. med. biol.*, vol. 41, pp. 2251–2269, 1996.

- [5] e. c. fear, s. c. hagness, p. m. meaney, m. okoniewski, and m. a. stuchly, "near-field imaging for breast tumor detection," *iee microwave mag.*, vol. 3, pp. 48–56, mar. 2002.
- [6] a. e. bulyshev, s. y. semenov, a. e. souvorov, r. h. svenson, a.g. nazarov, y. e. sizov, and g. p. tatsis, "computational modeling of three-dimensional microwave tomography of breast cancer," *iee trans. biomed. eng.*, vol. 48, pp. 1053–1056, sept. 2001.
- [7] d. li, p. m. meaney, and k. d. paulsen, "confocal microwave imaging for breast cancer detection," *iee trans. microwave theory tech.*, vol. 51, pp. 1179–1186, apr. 2003.
- [8] p. m. meaney, m. w. fanning, d. li, s. p. poplack, and k. d. paulsen, "a clinical prototype for active microwave imaging of the breast," *iee trans. microwave theory tech.*, vol. 48, pp. 1841–1853, nov. 2000.
- [9] s. c. hagness, a. taflove, and j. e. bridges, "two-dimensional ftd analysis of a pulsed microwave confocal system for breast cancer detection: fixed focus and antenna-array sensors," *iee trans. biomed. eng.*, vol. 45, pp. 1470–1479, dec. 1998.
- [10] "three-dimensional ftd analysis of a pulsed microwave confocal system for breast cancer detection: design of an antenna-array element," *iee trans. antennas propagat.*, vol. 47, pp. 783–791, may 1999.
- [11] x. li and s. c. hagness, "a confocal microwave imaging algorithm for breast cancer detection," *iee microwave guided wave lett.*, vol. 11, pp. 130–132, mar. 2001.
- [12] e. c. fear and m. a. stuchly, "microwave detection of breast cancer," *iee trans. microwave theory tech.*, vol. 48, pp. 1854–1863, nov. 2000.
- [13] e. c. fear, x. li, s. c. hagness, and m. a. stuchly, "confocal microwave imaging for breast tumor detection: localization in three dimensions," *iee trans. biomed. eng.*, vol. 49, pp. 812–822, aug. 2002.
- [14] e. c. fear, j. sill, and m. a. stuchly, "experimental feasibility study of confocal microwave imaging for breast tumor detection," *iee trans. microwave theory tech.*, vol. 51, pp. 887–892, mar. 2003.
- [15] e. j. bond, x. li, s. c. hagness, and b. d. van veen, "microwave imaging via space-time beamforming for early detection of breascancer," *iee trans. antennas propagat.*, vol. 51, pp. 1690–1705, aug. 2003.
- [16] x. li, s. c. hagness, b. d. van veen, and d. van der weide, "experimental investigation of microwave imaging via space-time beamforming for breast cancer detection," in *ieeemt-s int. microwave symp. dig.*, june 2003, pp. 379–382.
- [17] a. taflove and s. c. hagness, *computational electrodynamics: the finite-difference time-domain method*. boston, ma: artech house, 2000.
- [18] r. luebbers, f. hunsberger, k. kunz, r. standler, and m. schneider, "a frequency-dependent finite difference time domain formulation for dispersive materials," *iee trans. electromagn. compat.*, vol. 32, pp. 222–227, mar. 1990.
- [19] o. ghandi, "a frequency-dependent finite difference time domain formulation for general dispersive media," *iee trans. microwave theory tech.*, vol. 41, pp. 658–665, apr. 1993.
- [20] R. M. Joseph, S. C. Hagness, and A. Taflove, "Direct time integration of Maxwell's equations in linear dispersive media with absorption for scattering and propagation of femtosecond electromagnetic pulse," *Opt. Lett.*, vol. 16, pp. 1412–1414, sept. 1991.
- [21] D. M. Sullivan, "Z-transform theory and the FDTD method," *IEEE Trans. Antennas Propagat.*, vol. 55, pp. 28–34, Jan. 1996.
- [22] G. Fan and Q. H. Liu, "An FDTD algorithm with perfectly matched layers for general dispersive media," *IEEE Trans. Antennas Propagat.*, vol. 48, pp. 637–646, May 2000.
- [23] W. Weedon and C. Rappaport, "A general method for FDTD modeling of wave propagation in arbitrary frequency dispersive media," *IEEE Trans. Antennas Propagat.*, vol. 45, pp. 401–410, Mar. 1997.
- [24] C. Gabriel and S. Gabriel. *Compilation of the dielectric properties of body tissues at RF and microwave frequencies*. Brooks Air Force Base, Brooks AFB, OH. [Online]. Available: <http://www.brooks.af.mil/AFRL/HED/hedr/reports/dielectric>
- [25] C. Rappaport and S. Winton, "Modeling dispersive soil for FDTD computation by fitting conductivity parameters," in *12th Annu. Rev. Progress Applied Computational Electromagnetic Symp. Dig.*, Mar. 1997, pp. 112–118.
- [26] C. Rappaport, S. Wu, and S. Winton, "FDTD wave propagation in dispersive soil using a single pole conductivity model," *IEEE Trans. Magn.*, vol. 35, pp. 1542–1545, May 1999.
- [27] P. Kosmas, Y. Wang, and C. Rappaport, "Three-dimensional FDTD model for GPR detection of objects buried in realistic dispersive soil," in *Proc. SPIE*, vol. 4742, Orlando, FL, Apr. 2002, pp. 330–338.
- [28] C. Rappaport, E. Bishop, and P. Kosmas, "Modeling FDTD wave propagation in dispersive biological tissue using a single pole Z-transform function," in *IEEE Int. Engineering in Medicine and Biology Soc. Conf.*, Cancun, Mexico, Sept. 2003, pp. 3789–3792.
- [29] P. G. Petropoulos, "Stability and phase error analysis of FD-TD in dispersive dielectrics," *IEEE Trans. Antennas Propagat.*, vol. 42, pp. 62–69, Jan. 1994.
- [30] P. Kosmas and C. Rappaport, "A simple absorbing boundary condition for FDTD modeling of lossy, dispersive media based on the one-way wave equation," *IEEE Trans. Antennas Propagat.*, to be published.
- [31] S. D. Gedney, "An anisotropic perfectly matched layer-absorbing medium for the truncation of FDTD lattices," *IEEE Trans. Antennas Propagat.*, vol. 44, pp. 1630–1639, Dec. 1996.
- [32] , "An anisotropic PML absorbing media for the FDTD simulation of fields in lossy and dispersive media," *Electromagnetics*, vol. 16, pp. 399–415, 1996.
- [33] O. Ramadan and A. Y. Oztoprak, "Z-transform implementation of the perfectly matched layer for truncating FDTD domains," *IEEE Microwave Wireless Comp. Lett.*, vol. 13, pp. 402–404, Sept. 2003.
- [34] P. M. Meaney, private communication.
- [35] M. Doyley, private communication.
- [36] C. Rappaport and E. Bishop. *Microwave biological propagation models: Single pole time-domain dispersive media parameters*. Northeastern Univ., Boston, MA. [Online]. Available: <http://www.censsis.neu.edu/Research/R1/Modeling/>